Antifreeze proteins govern the precipitation of trehalose in a freezing-avoiding insect at low temperature

Xin Wen[a,b,1], Sen Wang[a,2], John G. Duman[c], Josh Fnu Arifin[a], Vonny Juwita[a], William A. Goddard III[b], Alejandra Rios[a,b,d], Fan Liu[b], Soo-Kyung Kim[b], Ravinder Abrol[b], Arthur L. DeVries[e], and Lawrence M. Henling[f]

[a]Department of Chemistry and Biochemistry, California State University, Los Angeles, CA 90032; [b]Division of Chemistry and Chemical Engineering, California Institute of Technology, Pasadena, CA 91125; [c]Department of Biological Sciences, University of Notre Dame, Notre Dame, IN 46556; [d]Department of Physics and Astronomy, California State University, Los Angeles, CA 90032; [e]Department of Animal Biology, University of Illinois at Urbana–Champaign, Urbana, IL 61801; and [f]Beckman Institute, California Institute of Technology, Pasadena, CA 91125

Edited by David L. Denlinger, Ohio State University, Columbus, OH, and approved April 28, 2016 (received for review January 30, 2016)

The remarkable adaptive strategies of insects to extreme environments are linked to the biochemical compounds in their body fluids. Trehalose, a versatile sugar molecule, can accumulate to high levels in freeze-tolerant and freeze-avoiding insects, functioning as a cryoprotectant and a supercooling agent. Antifreeze proteins (AFPs), known to protect organisms from freezing by lowering the freezing temperature and deferring the growth of ice, are present at high levels in some freeze-avoiding insects in winter, and yet, paradoxically are found in some freeze-tolerant insects. Here, we report a previously unidentified role for AFPs in effectively inhibiting trehalose precipitation in the hemolymph (or blood) of overwintering beetle larvae. We determine the trehalose level (29.6 ± 0.6 mg/mL) in the larval hemolymph of a beetle, *Dendroides canadensis,* and demonstrate that the hemolymph AFPs are crucial for inhibiting trehalose crystallization, whereas the presence of trehalose also enhances the antifreeze activity of AFPs. To dissect the molecular mechanism, we examine the molecular recognition between AFP and trehalose crystal interfaces using molecular dynamics simulations. The theory corroborates the experiments and shows preferential strong binding of the AFP to the fast growing surfaces of the sugar crystal. This newly uncovered role for AFPs may help explain the long-speculated role of AFPs in freeze-tolerant species. We propose that the presence of high levels of molecules important for survival but prone to precipitation in poikilotherms (their body temperature can vary considerably) needs a companion mechanism to prevent the precipitation and here present, to our knowledge, the first example. Such a combination of trehalose and AFPs also provides a novel approach for cold protection and for trehalose crystallization inhibition in industrial applications.

insects | environmental stress | trehalose | crystallization | antifreeze protein

Trehalose is a multifunctional nonreducing disaccharide, occurring naturally in all kingdoms (1–4). In addition to being an energy and carbon source, this sugar protects cells and proteins against injuries in extreme environments (1, 2, 4), prevents osteoporosis (5), alleviates certain diseases (6), and acts as a signal molecule in plants (7). Due to its bioprotective properties, trehalose is a potentially useful protectant of cells and proteins in numerous applications (2, 8). Its practical use, however, can be impaired by the fact that this sugar is prone to crystallization, in particular, when its aqueous solution is under fluctuating low temperatures. For example, the crystallization of trehalose dihydrate during the freeze-drying processes or from solutions at low temperatures would significantly jeopardize its ability to protect biomolecules (8–10). In comparison with other common sugars including sucrose, trehalose has a high propensity to crystallize at low temperature, forming trehalose dihydrate crystals. This propensity is due to: (*i*) the solubility of trehalose in water decreases dramatically or exponentially as temperature decreases (few data at low temperature were available, however) (11); (*ii*) trehalose dihydrate has a lower solubility than anhydrous trehalose in water (12); and (*iii*) the crystal structure of trehalose dihydrate lacks intramolecular hydrogen bonding (13). In nature, crystallization or solidification of physiological solutes in body fluids can be lethal. As the primary sugar in insects, trehalose is mainly stored in the hemolymph (14), and its production, however, can be induced to high levels in the winter hemolymph in response to harsh environmental stresses including low temperature (15, 16). Knowledge of the exact level of trehalose in winter hemolymph, whether this sugar crystallizes at such concentrations under fluctuating low temperatures, and the protection mechanism if it does not crystallize are essential for understanding cold survival strategies and for facilitating the development of medical and industrial applications of trehalose.

Antifreeze proteins (AFPs) bind to specific surfaces of ice crystals and inhibit their growth in the body fluids of cold-adapted organisms in vivo (17–21). AFPs depress the freezing point of water without appreciably altering the melting point leading to a difference between the melting point and the freezing point, referred to as thermal hysteresis (TH, a measure of antifreeze activity). AFPs in freeze-avoiding species (they die if frozen) prevent freezing in winter cold. However, they can also occur in freeze-tolerant species (those that survive if frozen) at levels too low to

Significance

Survival strategies for overwintering insects rely on the biochemical components in body fluids, where trehalose and antifreeze proteins (AFPs) are sometimes the best-known and extensively studied carbohydrate and protein components occurring in winters in both freeze-tolerant (they can survive if frozen) and freeze-avoiding species (they die if frozen). AFPs are known to lower the freezing temperature and defer the growth of ice, whereas their roles in freeze-tolerant species have long been speculated. By examining the larval blood of a freeze-avoiding beetle, we reveal a new role for AFPs by demonstrating that AFPs effectively inhibit trehalose crystallization. This finding provides a novel approach for cold protection and for inhibiting trehalose crystallization in medical and industrial applications.

Author contributions: X.W. and S.W. designed research; X.W. and S.W. initiated research; X.W. oversaw research; X.W., S.W., J.G.D., J.F.A., V.J., W.A.G., A.R., F.L., S.-K.K., R.A., A.L.D., and L.M.H. performed research; X.W., S.W., and W.A.G. analyzed data; and X.W., S.W., J.G.D., W.A.G., A.L.D., and L.M.H. wrote the paper.

The authors declare no conflict of interest.

This article is a PNAS Direct Submission.

Data deposition: The structures have been deposited at the Cambridge Crystallographic Data Centre, www.ccdc.cam.ac.uk/structures (CSD reference nos. 1053435 and 1053434).

[1]To whom correspondence should be addressed. Email: xwen3@calstatela.edu.

[2]Present address: Department of Chemistry, California State University, Dominguez Hills, Carson, CA 90747.

This article contains supporting information online at www.pnas.org/lookup/suppl/doi:10.1073/pnas.1601519113/-/DCSupplemental.

produce significant antifreeze activity, causing speculation as to their role in freeze-tolerant species (16). For example, the presence of AFPs in freeze-tolerant species is thought to prevent the damage caused by ice recrystallization (21). More recently, the control of the formation of crystals in addition to ice, including nucleosides and carbohydrates by AFPs, was reported in vitro (22–24), inspiring further exploration of other biological functions of AFPs, in particular, where dual functions have not been previously identified (15).

Dendroides canadensis, a pyrochroid beetle common in eastern North America (both Canada and the United States) (25), winter as larvae in multiple instars under the loose bark of partially decomposed hardwood logs. The overwintering larvae produce a family of some 30 AFP isomers (DAFPs) that are differentially expressed in various tissues and body fluids including hemolymph, gut, urine, and epidermal cells that function to prevent inoculative freezing and promote supercooling (26, 27). The DAFPs consist of 12- and 13-mer repeating units containing highly conserved threonine and cysteine residues (28, 29) that form a right-handed β-solenoid structure and a relatively flat ice-binding site on one side of the repeating β-strands (30). The combination of AFP isoforms, purging the gut of ice nucleating bacteria, and high concentrations of glycerol and other polyols permits the larvae to avoid freezing above temperatures of approximately −18 °C to −28 °C, depending on the severity of the winter (27). The hemolymph of *D. canadensis* was studied as a model system in this work.

Results

Determining the Trehalose Level in *D. canadensis* Hemolymph. To establish quantitatively the amount of trehalose in *D. canadensis* hemolymph, we first collected the winter and summer hemolymph of the beetle and determined the concentrations of trehalose in the hemolymph using trehalase. The level of trehalose was determined to be 29.6 ± 0.6 mg/mL or 0.09 M in the winter hemolymph, which is within the reported amounts of trehalose, ranging from 0.02 to 0.17 M, in insects (31). In contrast, the level of trehalose decreased dramatically to less than 0.1 mg/mL (or 0.3 mM) in the summer hemolymph as determined in this work. It is known that the solubility of trehalose in water changes dramatically with temperature and is exponentially low at low temperatures, but the data at low temperature are very few (11), which may be due to the difficulties in supercooling water during the experiments and measuring the solubility at low temperatures. Here, we were able to supercool water to −5 °C, −10 °C, and −15 °C during the experiments by using triple-filtered ultrapure water in extensively cleaned glass vials (*Materials and Methods*). We showed that when an aqueous solution of trehalose (29.6 mg/mL) was cooled and held at −5 °C with fluctuations within ±1 °C for 2 h, the precipitation of crystalline trehalose occurred (Fig. 1*A*). The sizes of these trehalose crystals increased continuously as the temperature was lowered to −10 °C and −15 °C (Fig. 1 *B* and *C*).

To demonstrate whether precipitates appear in the winter hemolymph of *D. canadensis*, similarly, we cooled and held the hemolymph sample to −5 °C, −10 °C, and −15 °C. As expected, no precipitates were observed in the normal winter hemolymph (Fig. 1 *D*–*F*). It was suggested that the high glass transition temperature of trehalose may lead to formation of a glassy matrix during cooling, preventing its crystallization. This vitrification hypothesis alone, however, may not be sufficient to explain why trehalose may remain soluble in the winter hemolymph because the solubility of trehalose in actual hemolymph would be lower than that in water (as the water activity is lower in such a complex system) and the winter temperatures typically fluctuate considerably over the winter, but are often higher than the glass transition temperature (9, 32–35). Such phase transitions of the hemolymph components are a potential cause of low temperature damage in freeze-avoiding insects (36). Hence, there must be some mechanisms that prevent trehalose crystallization in *D. canadensis* hemolymph during winter.

Trehalose Precipitates in DAFPs-Free Hemolymph. The concentrations of the four DAFP isomers with molecular weights ranging from 7 to 9 kDa are elevated in *D. canadensis* hemolymph in winter (1.6–2.6 mg/mL), resulting in high TH (or antifreeze) activity, whereas

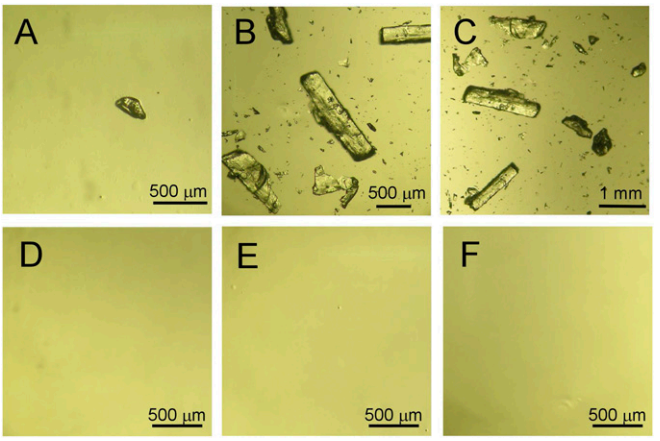

Fig. 1. Micrographs of trehalose aqueous solution and *D. canadensis* hemolymph during cooling and holding at low temperatures. Micrograph images of the aqueous solution of trehalose at 29.6 mg/mL (*A*–*C*) and the winter hemolymph of *D. canadensis* (*D*–*F*). (*A* and *D*) At −5 °C. (*B* and *E*) At −10 °C. (*C* and *F*) At −15 °C. Trehalose precipitates were observed in the trehalose aqueous solution but not *D. canadensis* hemolymph.

in contrast, their concentrations are too low to be measured in summer (37). It was reported that the antifreeze activity of pure DAFP can be further enhanced by trehalose at high, nonphysiological concentrations, such as 0.25 M or above (38). To explore the links between the inhibition of trehalose crystallization and the existence of DAFPs in the winter hemolymph, we removed DAFPs from the winter hemolymph by ultrafiltration (*Materials and Methods*) and performed similar experiments on the DAFPs-free hemolymph. In contrast to the normal hemolymph, crystalline precipitates appeared at −5 °C in the DAFPs-free hemolymph and the sizes of the precipitates increased when the temperature was lowered to −10 °C and −15 °C (Fig. 2 *A*–*C*). These precipitates were then collected and characterized using LC-MS spectrometry and NMR (^{1}H and ^{13}C) spectroscopy, which demonstrated that the crystalline precipitates were pure trehalose (Fig. 2 *D*–*F*).

Effects of DAFP-1 on Trehalose Crystallization. To validate that DAFPs are required for inhibiting trehalose crystallization in the hemolymph, we added purified DAFP-1 at 1.0 mg/mL (the most abundant hemolymph DAFP isoform at a physiological concentration) (37) back to the DAFPs-free hemolymph, where DAFPs were removed by ultrafiltration (*Materials and Methods*), and to a trehalose aqueous solution (29.6 mg/mL). No precipitates appeared in the DAFP-1–added hemolymph or trehalose solution when the sample solutions were cooled and held at −15 °C with fluctuations within ±1 °C for 2 h, suggesting that DAFP-1 blocks the nuclei of trehalose crystals. DAFP-1 has a molecular weight of about 9 kDa and 16 cysteine residues forming eight disulfide bonds that are crucial for its structure and function (22, 30). We denatured DAFP-1 by complete reduction of its disulfide bonds and used it as a control. In contrast, the addition of denatured DAFP-1 at the same or higher concentrations (up to 3.0 mg/mL) to the DAFPs-free hemolymph and to the trehalose solution, failed to inhibit the precipitation of crystalline trehalose that was observed in these samples at −5 °C.

To further understand the effect of DAFPs on trehalose crystallization, we investigated DAFP-1 as an additive. We first improved the crystallization conditions of trehalose to obtain well-formed trehalose dihydrate crystals by diffusing ethanol into trehalose aqueous ethanol solutions (Fig. 3*A*), where DAFP-1 was not denatured. We compared trehalose crystallization in the absence and presence of the DAFP additive. The presence of DAFP-1 at 0.04 mg/mL (or 5.0 μM) significantly delayed the first appearance of trehalose precipitates from day 4 to day 6 (Table 1) and resulted in much smaller final crystals (the median crystal size is reduced from 4,500 to 525 μm in

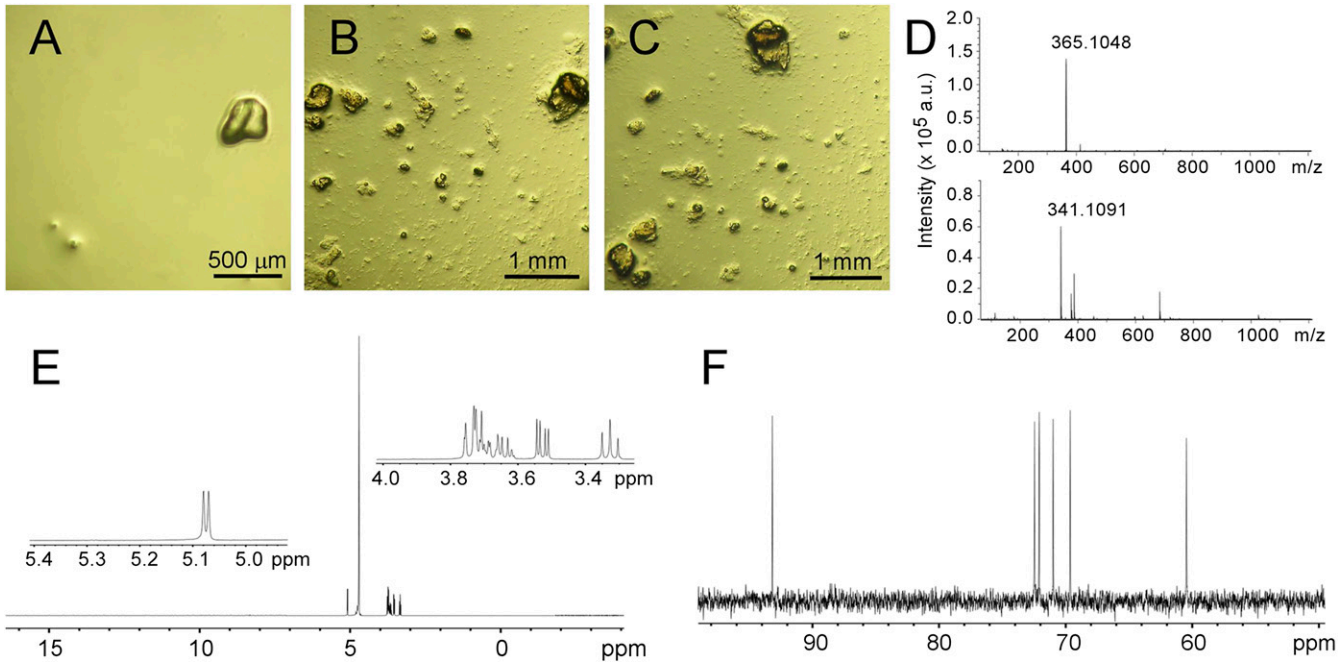

Fig. 2. The precipitates from the DAFPs-removed hemolymph, identified as trehalose. Micrograph images of the winter hemolymph of *D. canadensis* from which DAFPs were removed (*A*–*C*). (*A*) At −5 °C. (*B*) At −10 °C. (*C*) At −15 °C. Trehalose was identified in the precipitates from the DAFPs-removed hemolymph during cooling and holding at low temperatures: (*D*) by MS as indicated by the peak at *m/z* 365.1 in the positive ESI spectrum (*Upper*) and at *m/z* 341.1 in the negative ESI spectrum (*Lower*), and (*E* and *F*) by NMR spectroscopy as shown in the ^{1}H NMR spectrum (*E*) and the ^{13}C NMR spectrum (*F*).

the presence of DAFP-1) (Fig. 3*B*; see also Fig. S2). The higher the concentrations of DAFP-1, the more pronounced were the effects (Table 1 and Figs. S1 and S2). The crystals from these studies were confirmed to be trehalose dihydrate by single crystal X-ray diffraction, although the sizes of the trehalose crystals obtained in the absence and presence of DAFP-1 were different. The crystallographic data are summarized in Table S1. We interpret this by assuming that there are enough DAFP-1 molecules in the early stage of the experiments to block all of the critical nuclei of trehalose dihydrate crystals and inhibit the growth in the solutions. Here, the degrees of supersaturation of the trehalose solutions in the presence of DAFP-1 increase as time moves forward. When DAFP-1 molecules are consumed by previously formed nuclei in the solutions, new nuclei can now form and the nuclei (new or old) can now grow into trehalose dihydrate crystals without inhibition.

Moreover, we assessed the effect of trehalose on the TH of DAFP-1 at physiological concentrations. The TH of DAFP-1 at 1 mg/mL was assessed to be 5.59 °C, which can be enhanced ∼11% (to 6.20 °C) by 0.1 M trehalose (Fig. 4). The higher the concentration of trehalose, the more significant effect it has on the TH of the AFP. Note that the experiments described here were done using only DAFP-1 and trehalose in water, whereas hemolymph is a very complex system. These results suggest that trehalose also functions as a physiological antifreeze activity enhancer, working in cooperation with certain other solutes in the winter hemolymph to depress the freezing and supercooling points to sufficiently lower temperatures for *D. canadensis* wintering (39, 40).

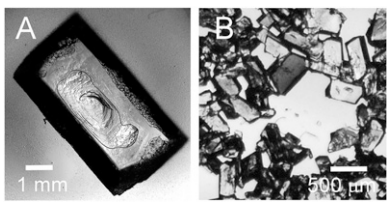

Fig. 3. Effects of DAFP-1 on trehalose crystallization. Micrographs of trehalose dihydrate crystals achieved in the absence of additives (*A*) and presence of DAFP-1 at 0.04 mg/mL (*B*).

Probing the Interactions Between DAFP-1 and Trehalose Dihydrate Crystals. To gain insights into the molecular recognition between DAFP-1 and trehalose dihydrate crystal surfaces, we performed molecular dynamics (MD) computational simulations to investigate the binding of DAFP-1 to two surfaces of trehalose dihydrate crystals: (−110) and (0–11). Compared with (0–11), (−110) is a relatively fast-growing surface (Fig. 5 *A* and *C*). The calculated surface energy (E_{surf}) of (−110) in the absence of DAFP-1 is about 4% higher than that of (0–11) (Table S2), which is consistent with the experimental data. On docking of DAFP-1, the calculated surface energies (E'_{surf}) of both (−110) and (0–11) significantly decrease, suggesting interactions between DAFP-1 and the surfaces. The E'_{surf} of (−110) is about 8% higher than that of (0–11), which is consistent with the observations that the size of trehalose dihydrate crystals became smaller in the presence of DAFP-1, whereas

Table 1. Inhibitory effects of varying concentrations of DAFP-1 on trehalose dihydrate crystallization

Sample*	DAFP-1 (mg/mL)	Induction time (d)†	Weight of crystals (mg)‡
Trehalose	NA	4	37.4 (0.1)
Trehalose + control	1.1	4	37.5 (0.1)
Trehalose + DAFP-1	0.04	6	28.2 (0.1)
Trehalose + DAFP-1	0.1	8	17.9 (0.1)
Trehalose + DAFP-1	0.8	8	15.6 (0.2)

NA, not available.
*Each sample contained 39.0 ± 0.0 mg trehalose on day 1, and the experiments were stopped on day 21. Results of trehalose alone and in the presence of control (i.e., denatured DAFP-1) are listed for comparison.
†The day that the first appearance of solid was observed.
‡SDs are given in parentheses after the means. The crystal size distributions are shown in Fig. S2.

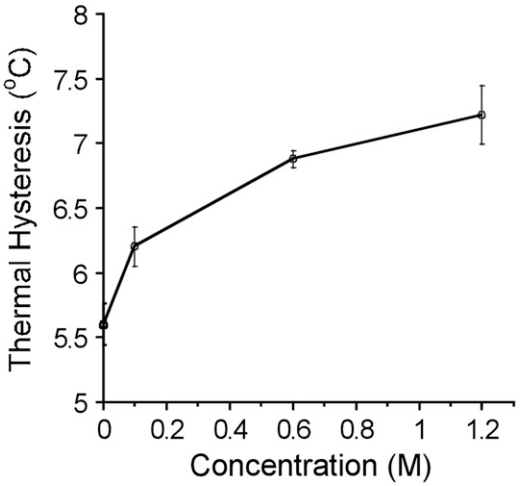

Fig. 4. Thermal hysteresis activities of DAFP-1 (1 mg/mL) in the absence and presence of trehalose at various concentrations. The SDs from at least three measurements are shown as the error bars.

the shape had no apparent change. The binding of DAFP-1 to both surfaces ($\Delta\Delta E_{bind}$) is energetically favorable and results in the reduction of surface energies of both surfaces by about 40% (Table S2). In addition, we found hydrogen bonding interactions mainly between the conserved threonines on the putative flat ice-binding surface of DAFP-1 and trehalose or water molecules on the trehalose dihydrate crystalline surfaces (Table S3). Because of the curvature of (0–11) surface, there are about 40% fewer hydrogen bonds at the interface between DAFP-1 and the (0–11) face than those between DAFP-1 and the (−110) face (Table S3). The theory shows preferential strong binding of the protein to the fast growing surfaces of the sugar crystal. The results support that DAFP-1 blocks the growth surfaces of the critical nuclei of trehalose dihydrate crystal.

Discussion

Our data here provide evidence on high levels of trehalose in conjunction with an inhibitory strategy of trehalose crystallization in winter hemolymph of *D. canadensis*. We demonstrate that the presence of AFPs is essential to prevent trehalose precipitation in *D. canadensis* hemolymph under fluctuating low temperatures and trehalose may also function as a physiological enhancer for the antifreeze activity of AFPs. We reveal a previously unidentified role for the AFPs in inhibiting trehalose crystallization, probably through blocking the nuclei of trehalose dihydrate crystals, and show that such inhibitory efficiency of the AFPs is high. In contrast to the physiological concentration for its antifreeze role (1 mg/mL), only 0.04 mg/mL (or about 25 times less) is needed to effectively delay the precipitation of trehalose. Our computational simulation data support the experimental data and suggest that interactions between the putative ice-binding surface of DAFP-1 and specific trehalose dihydrate crystal surfaces are important for such recognition. This finding suggests that as proto-nuclei form, the protein binds to the fast growing surfaces preventing this proto-nucleus from growing into a crystal. These proto-nuclei are too small to see experimentally. This situation persists, with additional proto-nuclei forming but stopped from growing until the supply of protein is exhausted. As a result, no crystals are observed. Eventually, when protein is exhausted all the proto-nuclei that have been inhibited start growing at the same time so that the resulting crystals are all similar in size. Other freeze-avoiding beetles have AFPs structurally similar to the DAFPs (19, 40), and consequently their AFPs are also likely to prevent trehalose crystallization. Other insect AFPs are structurally different (19) and, although these may also inhibit trehalose crystallization, this remains to be proven.

As an effective cryoprotectant, trehalose plays an important role in stabilizing proteins and protecting cell membranes in freeze-tolerant insects (15). The problem of trehalose crystallization is likely to be more problematic in freeze-tolerant insects. Induced generally by extracellular ice-nucleating agents, ice formation in freeze-tolerant species is usually restricted to the extracellular fluid. Consequently, the concentrations of trehalose and other nonpenetrating hemolymph solutes may increase severalfold depending on the extent of freezing, thereby exacerbating the hemolymph solute crystallization potential.

The AFPs responsible for the low TH activities of freeze-tolerant insects have not been characterized, and consequently it is not currently possible to examine their trehalose crystallization inhibition ability. The one exception is actually *D. canadensis*. Although *D. canadensis* have been freeze avoiding in northern Indiana since the 1980s (40, 41), during the very cold winters in the 1970s, they were freeze-tolerant (42), and consequently, the DAFPs may have played an even more important role in inhibiting trehalose crystallization. In addition, antifreeze glycolipids with TH activity similar to insect AFPs have been characterized from freeze-tolerant insects, frogs, and plants (43, 44). It is possible that these glycolipids also inhibit trehalose crystallization.

Moreover, as a highly stable, multifunctional disaccharide, trehalose not only has many distinct physiological roles in organisms but also industrial applications in pharmaceutical and food industries where the high propensity of trehalose to crystallize to trehalose dihydrate can deteriorate the quality of certain products. Consequently, DAFP-like AFPs, and very probably other AFPs, may effectively eliminate this problem.

In summary, our work reveals a significant synergistic relationship between trehalose and AFPs in cold protection, suggesting a new role for AFPs that yields further insights into cold survival strategy. This finding suggests new approaches toward designing cryoprotective systems and new, improved industrial uses for trehalose in the presence of AFPs.

Materials and Methods

Materials. All chemicals were purchased from Sigma-Aldrich at ACS grade or better and were used without additional purification. HPLC-grade solvents and chemicals were purchased from Sigma-Aldrich. All of the aqueous solutions were prepared using Milli-Q water produced from a Synergy water system (Millipore) with a minimum resistivity of 18 MΩ·cm. All of the samples including the protein samples were filtered through 0.2-μm filters before use unless otherwise indicated. Sample vials (National Scientific; 8 mL) were cleaned as previously described (22) and then used for crystallization.

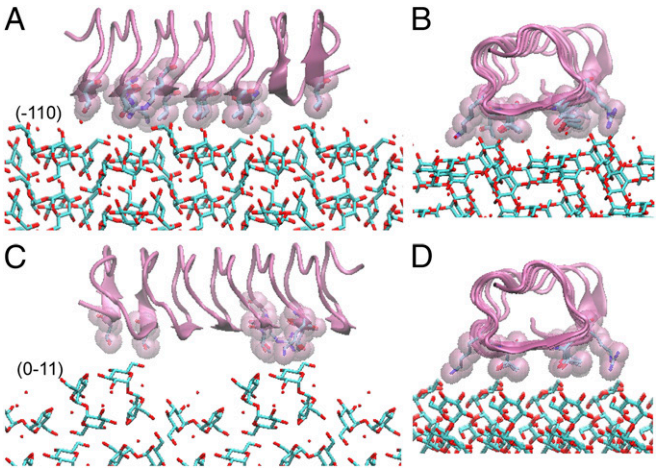

Fig. 5. Model of DAFP-1 binding to trehalose dihydrate (−110) and (0–11) surfaces. Side views of showing the hydrogen bonding network between DAFP-1 and (−110) (*A* and *B*: the two views are related by a 90° rotation around the vertical axis] and between DAFP-1 and (0–11) (*C* and *D*: the two views are related by a 90° rotation around the vertical axis). Trehalose dihydrate is shown in licorice. DAFP-1 is represented as a cartoon in pale purple and the residues forming hydrogen bonds with the sugar molecules on the crystal surface are represented as van der Waals spheres with licorice inside.

AFP and Control Preparation. DAFP-1 was expressed and purified as described previously (38). The purified DAFP-1 was characterized using SDS/PAGE gel electrophoresis, MALDI-TOF MS, circular dichroism (CD) spectrometry, and differential scanning calorimetry (DSC), as previously described (30), and the identity of DAFP-1 was confirmed. The concentration of stock DAFP-1 solution was determined using a Cary 100 Bio UV-Vis spectroscopy (Varian), and the extinction coefficient of 5.47×10^3 $M^{-1} \cdot cm^{-1}$ at 280 nm was used (45). All of the weight measurements were carried out with an Ohaus Voyager Pro analytical and precision balance. The denatured DAFP-1 with completely reduced disulfide bonds was prepared following the previously reported methods (46). To fully reduce all of the disulfide bonds in DAFP-1, purified DAFP-1 (~1 mM) was incubated in 0.10 M sodium citrate, pH 3.0, and 15.0 mM Tris(2-carboxyethyl)phosphine hydrochloride (TCEP) at 60 °C for 30 min. Then the denatured DAFP-1 was further purified using ÄKTA Purifier 10 (GE Healthcare) with a Sephacryl S-100 gel filtration column (GE Healthcare).

Preparation of *D. canadensis* Hemolymph. Larvae were collected in the field from wooded areas in the vicinity of South Bend, Indiana (northern Indiana and southern Michigan) in both summer (July) and winter (January). Larvae were kept at field temperatures and immediately transported to the laboratory at the University of Notre Dame where hemolymph was extracted from individual larvae by puncturing the cuticle in the dorsal midline with a 30-gauge needle and collecting the hemolymph (~2–8 μL per individual) in a 10-μL glass capillary tube via capillary action. Hemolymph was pooled and stored at −80 °C.

Determination of the Levels of Trehalose in the Hemolymph of *D. canadensis*. The amount of trehalose in the hemolymph of *D. canadensis* was determined using a modified method (47, 48). The hemolymph, 5 μL, was placed in a polyethylene centrifuge tube containing 195 μL 0.25 M Na_2CO_3. The sample was vortexed for 2 min and then incubated at 100 °C for 3 h to inactivate all enzymes in the hemolymph and to convert glucose, if any, into its reductive form. The pH of the sample was adjusted to 5.70 by adding 960 μL 1 M acetic acid and 3.84 mL 0.25 M sodium acetate. The sample was then centrifuged at 13,800 × *g* at 25 °C for 10 min. To fully convert trehalose in the hemolymph into glucose, 100 μL of the supernatant was incubated overnight at 37 °C with 2 μL porcine kidney trehalase (Sigma; T8778). The amount of glucose in 46 μL of the treated supernatant was measured using the Glucose Assay Kit (Sigma; GAGO20). The glucose concentration was corrected by deducting the amount of glucose present in the supernatant before trehalase treatment. Concentrations were extrapolated from calibration standard curves using six standard concentrations. The experiments were repeated three times, each time in five replicates. The data are presented as mean ± SD.

In Vitro Beetle Hemolymph Experiments. The sizes of winter hemolymph DAFP isomers are between 7 and 9 kDa. Forty microliters of winter hemolymph was diluted to 200 μL by adding 160 μL of double deionized water. A 100-μL aliquot of the diluted hemolymph was passed through the Nanosep Centrifugal Devices (Pall Corporation; MWCO 3K) and the filtrate, which yielded a filtrate free of hemolymph macromolecules including DAFPs, was saved for use. A second 100-μL aliquot of the diluted hemolymph portion of the hemolymph was passed through Nanosep Centrifugal Devices (Pall Corporation; MWCO 10K), and the samples on the ultrafiltration membrane and in the sample reservoir, if any, were recovered and saved for use. The two saved samples were combined and lyophilized. The lyophilized sample was then solubilized in 40 μL deionized water, yielding a DAFPs-free hemolymph sample. Forty microliters of the following samples, native winter beetle hemolymph (vial 1), the DAFPs-free hemolymph sample (vial 2), and a 29.6 mg/mL trehalose aqueous solution (vial 3, a control), were placed in three vials, respectively. The sample vials were then placed into the center of aluminum blocks of a bench top hot/cold block incubator (TropiCooler; Boekel Scientific). The temperature was cooled from room temperature to −5 °C and held for 2 h. Images were then taken for the samples at −5 °C. The temperature was then cooled to −10 °C and held for 2 h. Images were then taken for the samples at −10 °C. The temperature was then cooled to −15 °C and held for 2 h. Images were then taken for the samples at −15 °C. The hemolymph experiments were repeated twice independently. The control experiment was repeated five times. The cooling rate was 1 °C/min for the above experiments. The solids that appeared in vial 2 were collected and washed three times with cold 70% (vol/vol) ethanol-water solution at −20 °C. The solid samples were held under vacuum for 24 h.

Mass Spectrometry. Mass spectra of the solid samples were obtained using a Waters 2795 HPLC system with ZQ single quadrupole MS and an electrospray ionization (ESI) source. Samples were introduced using loop injection. The results of the mass spectra of the vial 2 sample are shown as follows: positive ESI, *m/z*: $[M + Na]^+$ calculated for $C_{12}H_{22}O_{11}Na$, 365.33; found 365.11; negative ESI, *m/z*: $[M - H]^-$ calculated for $C_{12}H_{22}O_{11}Na$, 341.33; found 341.11.

NMR Spectroscopy. Bruker 400 NMR spectrometry was used to acquire ^1H NMR (D_2O, 400 NMR) and ^{13}C NMR (D_2O, 100.6 NMR). The ^1H and ^{13}C NMR spectra of the sample in vial 2 are identical to the standard spectra of D-trehalose dihydrate deposited in biological magnetic resonance data bank (BMSE 000125).

Crystal Growth Procedure and Size Analysis. Trehalose can be crystallized (dihydrate form) from pyridine or aqueous solutions of ethanol by evaporation (49, 50). However, we found that the single crystal yield was low: 30% from pyridine-ethanol solutions and 5% from aqueous ethanol solutions. Here, we crystallized trehalose dihydrate crystals by diffusing ethanol into the aqueous ethanol solution of trehalose directly. D-(+)-trehalose, 0.429 g, was dissolved into 3.30 mL water at 29 °C, and then 6.6 mL anhydrous ethanol was added. On day 1, each sample vial was weighed, and 900 μL of the above alcoholic trehalose solution was added. Then, 3 μL of water or protein solutions at certain concentrations were added into each vial. The vials were gently swirled after the addition and were transferred into a big jar containing ethanol to a depth of about 2 cm. The final trehalose concentration was 125 mM in each vial, and the protein/trehalose molar ratios ($\times 10^{-4}$) were varied at 0, 0.05, 0.5, 1.2, 1.5, 7.2, and 9.0. The cover of the jar was closed tightly, and the jar was held at 4 °C. Each vial was checked for crystals every 8 h until crystals appeared. The solution in each vial was then removed on day 21. The weights of the crystals were measured on day 43, and the resulting crystals were examined using a polarized microscope and single crystal X-ray diffraction. After the vials were dried in the air, the weight for each vial with the crystals was recorded. The experiments were repeated five times. The single crystal yield was 100% using the diffusion method. The crystal size analysis was performed by measuring the maximum length of the achieved crystals, and size distributions of trehalose dihydrate crystals in the absence and presence of varying concentrations of DAFP-1 are plotted in Fig. S2. Photographs of the vials were taken with a Canon EOS 30D camera during and at the end of the crystallization process and when the process finished. Optical micrographs were taken under a Nikon SMZ800 microscope with a Nikon Coolpix 5400 when the crystallization was completed.

Thermal Hysteresis Measurements. Freezing and melting points were determined in aqueous samples using a Clifton nanolitre osmometer (Clifton Technical Physics) following a previously reported protocol (51). The instrument was calibrated with distilled water (0 mOsm) and a 1,000 mOsm NaCl standard (Optimole; Wescor). Samples were suspended in heavy immersion oil. They were cooled until frozen and then slowly warmed until a single ice crystal (~15–20 μm) slowly melted while observed at 200×. This temperature was taken as the melting point or equilibrium freezing point. Following determination of the melting point, a 10-μm single ice crystal was slowly cooled to 0.18 °C below the melting point held for 1 min and then cooled to 1.8 °C and held for 1 min, then 3.6 °C for 1 min, then 5.4 °C, and then held at −6 °C for 30 min. They were then cooled at 0.074 °C/min until sudden rapid growth was observed, and this value was taken as the hysteresis freezing point. Melting and freezing point determinations for each sample were repeated at least three times. The thermal hysteresis, the difference between the melting point and the freezing point, represents the antifreeze activity.

MD Simulation Methods. The starting 3D structure of DAFP-1 and the denatured DAFP-1 were created from a homology model of a *Tenebrio molitor* AFP, TmAFP (PDB ID code 1EZG) (30, 52). There are eight disulfide bonds in DAFP-1, whereas all of the disulfide bonds in the denatured DAFP-1 are reduced. After energy minimizations, the structures of DAFP-1 and the denatured DAFP-1 were simulated as described previously (30), and the final snapshots were taken as the equilibrated structures (Fig. S3). The stability of the DAFP-1 model was validated by performing MD simulations and analyzing the backbone RMSD values relative to those of TmAFP (*SI Materials and Methods* and Figs. S4 and S5). A fast-growing surface, (−110), and a relatively slow-growing surface, (0–11), of the trehalose dihydrate crystal were then investigated. The slabs of (−110) and (0–11) trehalose dihydrate crystal surfaces were constructed using Cerius^2 (Accelrys) from $4 \times 4 \times 4$ and $8 \times 3 \times 3$ supercells, respectively. The surface energies (E_{surf}) were computed as $E_{surf} = [E_{slab} - (N_{slab}/N_{bulk})E_{bulk}]/2A$, where E_{slab} is the potential energies of the surface slab and the bulk unit cell in vacuum at 0 K, respectively, N_{slab} and N_{bulk} are the number of molecules in the slab and the bulk unit cell, respectively, and A is the area of the surface unit cell (53). DAFP-1 and denatured DAFP-1 were manually docked on the (−110) and (0–11) surfaces of trehalose dihydrate by maximizing hydrogen bonding interactions between the protein and the molecules on the specific crystal surface of trehalose dihydrate, respectively. The systems (protein and slab) were minimized in vacuum using the Assisted Model Building with Energy Refinement (AMBER) force field. Relative binding energies $\Delta\Delta E_{bind}$ of DAFP-1 to the surfaces were calculated as $\Delta\Delta E_{bind} = \Delta E_{system1} - \Delta E_{system2}$ where $\Delta E_{system} = E_{system} - (E_{protein} + E_{slab})$, and systems 1 and 2 refer to the systems containing WT DAFP-1 and denatured DAFP-1, respectively.

Single Crystal X-Ray Diffraction. Diffraction data (ϕ- and ω-scans) were collected at low temperature (100 K) on a Bruker AXS KAPPA APEX II CCD diffractometer with graphite monochromated Mo K_α radiation ($\lambda = 0.71073$ Å) at the California Institute of Technology's X-Ray Crystallography Facility. The structure was solved by direct methods using XT (54) and refined against F^2 on all data by full-matrix least squares with SHELXL-2014. All nonhydrogen atoms were refined anisotropically; all hydrogen atoms were refined isotropically. The crystallographic data of trehalose dihydrate crystals grown in the presence of DAFP-1 are summarized in Table S1. The structures reported in this paper have been deposited at the Cambridge Crystallographic Data Centre as CSD reference nos. 1053435 and 1053434.

More information on concentration effects of DAFP-1 on trehalose crystallization, crystallographic data for trehalose crystals, modeled structures of WT and denatured DAFP-1, calculated surface energies of trehalose dihydrate and relative binding energies of DAFP-1 to these surfaces, and potential hydrogen bonding interactions between DAFP-1 and trehalose dihydrate crystals are provided in *SI Materials and Methods*. Datasets S1 and S2 contain the supplementary crystallographic data for this paper. These data can be obtained free of charge from The Cambridge Crystallographic Data Centre via www.ccdc.cam.ac.uk/structures.

ACKNOWLEDGMENTS. This work was supported by National Institutes of Health Grant GM086249 (to X.W.). The Bruker KAPPA APEXII X-ray diffractometer was purchased via a National Science Foundation (NSF) Chemistry Research Instrumentation and Facilities: Departmental Multiuser Instrumentation (CRIF:MU) award to the California Institute of Technology (Caltech) (CHE-0639094). W.A.G. thanks NSF (EFRI-1332411) for support of Caltech theory efforts in this project. A.R. thanks Caltech Minority Undergraduate Research Fellowships funded by the Howard Hughes Medical Institute. The LC-MS was supported by National Center for Research Resources Grant S10-RR025631 to the University of California, Los Angeles, where Dr. Greg Khitrov provided assistance.

1. Crowe JH (2007) *Tehalose as a "Chemical Chaperone."* (Springer, New York), pp 146–158.
2. Elbein AD, Pan YT, Pastuszak I, Carroll D (2003) New insights on trehalose: A multifunctional molecule. *Glycobiology* 13(4):17R–27R.
3. Gibney PA, Schieler A, Chen JC, Rabinowitz JD, Botstein D (2015) Characterizing the in vivo role of trehalose in *Saccharomyces cerevisiae* using the AGT1 transporter. *Proc Natl Acad Sci USA* 112(19):6116–6121.
4. Kandror O, DeLeon A, Goldberg AL (2002) Trehalose synthesis is induced upon exposure of *Escherichia coli* to cold and is essential for viability at low temperatures. *Proc Natl Acad Sci USA* 99(15):9727–9732.
5. Nishizaki Y, et al. (2000) Disaccharide-trehalose inhibits bone resorption in ovariectomized mice. *Nutr Res* 20(5):653–664.
6. Sarkar S, Davies JE, Huang Z, Tunnacliffe A, Rubinsztein DC (2007) Trehalose, a novel mTOR-independent autophagy enhancer, accelerates the clearance of mutant huntingtin and α-synuclein. *J Biol Chem* 282(8):5641–5652.
7. Satoh-Nagasawa N, Nagasawa N, Malcomber S, Sakai H, Jackson D (2006) A trehalose metabolic enzyme controls inflorescence architecture in maize. *Nature* 441(7090):227–230.
8. Ohtake S, Wang YJ (2011) Trehalose: Current use and future applications. *J Pharm Sci* 100(6):2020–2053.
9. Sundaramurthi P, Suryanarayanan R (2010) Trehalose crystallization during freeze-drying: Implications on lyoprotection. *J Phys Chem Lett* 1(2):510–514.
10. Sundaramurthi P, Patapoff TW, Suryanarayanan R (2010) Crystallization of trehalose in frozen solutions and its phase behavior during drying. *Pharm Res* 27(11):2374–2383.
11. Chen T, Fowler A, Toner M (2000) Literature review: Supplemented phase diagram of the trehalose-water binary mixture. *Cryobiology* 40(3):277–282.
12. Sundaramurthi P, Suryanarayanan R (2010) Influence of crystallizing and non-crystallizing cosolutes on trehalose crystallization during freeze-drying. *Pharm Res* 27(11):2384–2393.
13. Jeffrey GA (1973) Intramolecular hydrogen-bonding in carbohydrate crystal-structures. *Carbohydr Res* 28(2):233–241.
14. Nation JL (2008) *Insect Physiology and Biochemistry* (CRC Press, Boca Raton, FL), 2nd Ed.
15. Denlinger DL, Lee, Jr RE, eds (2010) *Low Temperature Biology of Insects* (Cambridge Univ Press, New York).
16. Bale JS (2002) Insects and low temperatures: From molecular biology to distributions and abundance. *Philos Trans R Soc Lond B Biol Sci* 357(1423):849–862.
17. DeVries AL (1971) Glycoproteins as biological antifreeze agents in antarctic fishes. *Science* 172(3988):1152–1155.
18. Yeh Y, Feeney RE (1996) Antifreeze proteins: Structures and mechanisms of function. *Chem Rev* 96(2):601–618.
19. Davies PL (2014) Ice-binding proteins: A remarkable diversity of structures for stopping and starting ice growth. *Trends Biochem Sci* 39(11):548–555.
20. Raymond JA, DeVries AL (1977) Adsorption inhibition as a mechanism of freezing resistance in polar fishes. *Proc Natl Acad Sci USA* 74(6):2589–2593.
21. Knight CA, DeVries AL, Oolman LD (1984) Fish antifreeze protein and the freezing and recrystallization of ice. *Nature* 308(5956):295–296.
22. Wang S, Wen X, Nikolovski P, Juwita V, Arifin JF (2012) Expanding the molecular recognition repertoire of antifreeze polypeptides: Effects on nucleoside crystal growth. *Chem Commun (Camb)* 48(94):11555–11557.
23. Wang S, Wen X, Golen JA, Arifin JF, Rheingold AL (2013) Antifreeze protein-induced selective crystallization of a new thermodynamically and kinetically less preferred molecular crystal. *Chemistry* 19(47):16104–16112.
24. Wang S, et al. (2014) Molecular recognition of methyl α-D-mannopyranoside by antifreeze (glyco)proteins. *J Am Chem Soc* 136(25):8973–8981.
25. Young DK (1975) A revision of the family Pyrochroidae (Coleoptera, Heteromera) for North America, based on the larvae, pupae, and adults. *Contrib Am Entomol Inst* 11:1–39.
26. Duman JG, Verleye D, Li N (2002) Site-specific forms of antifreeze protein in the beetle *Dendroides canadensis*. *J Comp Physiol B* 172(6):547–552.
27. Nickell PK, Sass S, Verleye D, Blumenthal EM, Duman JG (2013) Antifreeze proteins in the primary urine of larvae of the beetle *Dendroides canadensis*. *J Exp Biol* 216(Pt 9):1695–1703.
28. Duman JG, et al. (1998) Molecular characterization and sequencing of antifreeze proteins from larvae of the beetle *Dendroides canadensis*. *J Comp Physiol B* 168(3):225–232.
29. Andorfer CA, Duman JG (2000) Isolation and characterization of cDNA clones encoding antifreeze proteins of the pyrochroid beetle *Dendroides canadensis*. *J Insect Physiol* 46(3):365–372.
30. Wang S, et al. (2009) Arginine, a key residue for the enhancing ability of an antifreeze protein of the beetle *Dendroides canadensis*. *Biochemistry* 48(40):9696–9703.
31. Blum MS ed (1985) *Fundamentals of Insect Physiology* (Wiley-Interscience, New York), 1st Ed.
32. Crowe JH, Carpenter JF, Crowe LM (1998) The role of vitrification in anhydrobiosis. *Annu Rev Physiol* 60(1):73–103.
33. Fedorov MV, Goodman JM, Nerukh D, Schumm S (2011) Self-assembly of trehalose molecules on a lysozyme surface: The broken glass hypothesis. *Phys Chem Chem Phys* 13(6):2294–2299.
34. Willart JF, et al. (2006) Metastability release of the form alpha of trehalose by isothermal solid state vitrification. *J Phys Chem B* 110(23):11040–11043.
35. Cardona S, Schebor C, Buera MP, Karel M, Chirife J (1997) Thermal stability of invertase in reduced-moisture amorphous matrices in relation to glassy state and trehalose crystallization. *J Food Sci* 62(1):105–112.
36. Ramløv H (2000) Aspects of natural cold tolerance in ectothermic animals. *Hum Reprod* 15(Suppl 5):26–46.
37. Duman JG, Serianni AS (2002) The role of endogenous antifreeze protein enhancers in the hemolymph thermal hysteresis activity of the beetle *Dendroides canadensis*. *J Insect Physiol* 48(1):103–111.
38. Amornwittawat N, et al. (2009) Effects of polyhydroxy compounds on beetle antifreeze protein activity. *Biochim Biophys Acta* 1794(2):341–346.
39. Wen X, Wang S, Amornwittawat N, Houghton EA, Sacco MA (2011) Interaction of reduced nicotinamide adenine dinucleotide with an antifreeze protein from *Dendroides canadensis*: Mechanistic implication of antifreeze activity enhancement. *J Mol Recognit* 24(6):1025–1032.
40. Duman JG (2015) Animal ice-binding (antifreeze) proteins and glycolipids: An overview with emphasis on physiological function. *J Exp Biol* 218(Pt 12):1846–1855.
41. Horwath KL, Duman JG (1984) Yearly variations in the overwintering mechanism of the cold hardy beetle *Dendroides canadensis*. *Physiol Zool* 57(1):40–45.
42. Duman JG (1980) Factors involved in the overwintering survival of the freeze tolerant beetle, *Dendroides canadensis*. *J Comp Physiol B* 136(1):53–59.
43. Walters KR, Jr, Serianni AS, Sformo T, Barnes BM, Duman JG (2009) A nonprotein thermal hysteresis-producing xylomannan antifreeze in the freeze-tolerant Alaskan beetle *Upis ceramboides*. *Proc Natl Acad Sci USA* 106(48):20210–20215.
44. Walters KR, Jr, et al. (2011) A thermal hysteresis-producing xylomannan glycolipid antifreeze associated with cold tolerance is found in diverse taxa. *J Comp Physiol B* 181(5):631–640.
45. Pace CN, Vajdos F, Fee L, Grimsley G, Gray T (1995) How to measure and predict the molar absorption coefficient of a protein. *Protein Sci* 4(11):2411–2423.
46. Li N, Chibber BAK, Castellino FJ, Duman JG (1998) Mapping of disulfide bridges in antifreeze proteins from overwintering larvae of the beetle *Dendroides canadensis*. *Biochemistry* 37(18):6343–6350.
47. Parrou JL, François J (1997) A simplified procedure for a rapid and reliable assay of both glycogen and trehalose in whole yeast cells. *Anal Biochem* 248(1):186–188.
48. Huang J-H, Lee H-J (2011) RNA interference unveils functions of the hypertrehalosemic hormone on cyclic fluctuation of hemolymph trehalose and oviposition in the virgin female *Blattella germanica*. *J Insect Physiol* 57(7):858–864.
49. Taga T, Senma M, Osaki K (1972) The crystal and molecular structure of trehalose dihydrate. *Acta Crystallogr B* 28(11):3258–3263.
50. Brown GM, et al. (1972) The crystal structure of α,α-trehalose dihydrate from three independent X-ray determinations. *Acta Crystallogr B* 28(11):3145–3158.
51. Cziko PA, Evans CW, Cheng C-HC, DeVries AL (2006) Freezing resistance of antifreeze-deficient larval Antarctic fish. *J Exp Biol* 209(Pt 3):407–420.
52. Liou Y-C, Tocilj A, Davies PL, Jia Z (2000) Mimicry of ice structure by surface hydroxyls and water of a β-helix antifreeze protein. *Nature* 406(6793):322–324.
53. Ludwig J, Vlachos DG, van Duin ACT, Goddard WA, 3rd (2006) Dynamics of the dissociation of hydrogen on stepped platinum surfaces using the ReaxFF reactive force field. *J Phys Chem B* 110(9):4274–4282.
54. Sheldrick GM (1990) Phase annealing in SHELX-90: Direct methods for larger structures. *Acta Crystallogr A* 46:467–473.
55. Phillips JC, et al. (2005) Scalable molecular dynamics with NAMD. *J Comput Chem* 26(16):1781–1802.
56. Case DA (2002) Amber and its associated force fields: An update. *Abstr Pap Am Chem Soc* 223:U475.
57. Jorgensen WL, Chandrasekhar J, Madura JD, Impey RW, Klein ML (1983) Comparison of simple potential functions for simulating liquid water. *J Chem Phys* 79(2):926–935.
58. Humphrey W, Dalke A, Schulten K (1996) VMD: Visual molecular dynamics. *J Mol Graph* 14(1):33–38, 27–28.